

# **High-Pressure Induced Reentrant Electronic and Magnetic State in $\text{Pr}_{0.7}\text{Ca}_{0.3}\text{MnO}_3$ Manganite**

Congwu Cui and Trevor A. Tyson

Physics Department, New Jersey Institute of Technology, Newark, New Jersey 07102

## **ABSTRACT**

In  $\text{Pr}_{0.7}\text{Ca}_{0.3}\text{MnO}_3$ , pressure induces reentrant magnetic and electronic state changes in the range 1atm to  $\sim 6$  GPa. The metal-insulator and magnetic transition temperatures coincide from  $\sim 1$  to 5 GPa, decouple outside of this range and do not change monotonically with pressure. The effects may be explained by competition between double exchange and super exchange. The insulating state below  $\sim 0.8$  GPa is ferromagnetic (FM) and antiferromagnetic phase-separated while possibly FM above  $\sim 5$  GPa. Charge ordering is suppressed and at high pressures an unusual paramagnetic insulating state is induced.

PACS Numbers: 62.50.+p, 71.27.+a, 71.30.+h, 75.47.Lx

The colossal magnetoresistive (CMR) manganite  $\text{Pr}_{1-x}\text{Ca}_x\text{MnO}_3$  is a narrow bandwidth system due to the large mismatch between the Pr, Ca and Mn ion sizes. The transfer integral is small and consequently in the whole doping range, the  $e_g$  electrons are localized. In the  $x = 0.3$  compound, a charge ordering (CO) transition occurs at  $\sim 220$  K, upon further cooling, an antiferromagnetic (AFM) ordering state arises at  $\sim 130$  K and a ferromagnetic (FM) state becomes evident at  $\sim 115$  K [1]. In the neutron diffraction pattern at low temperature, it was found that there are two sets of magnetic lines: ferromagnetic ones, as in the  $x = 0.2$  case and antiferromagnetic ones, similar to that in  $x = 0.4$  compound. Hence it is probable that two phases coexist at low temperature [1]. This compound is particularly interesting because of the intriguing phenomena: magnetic [2], high electric fields [3], irradiation with x-rays [4, 5] or visible light [6] can all destroy the CO state and lead to a conducting state.

In the magnetic field induced insulator-to-metal transition, the charge ordered insulating (COI) state is melted, simultaneously, the magnetic state also change from paramagnetic (PM) or AFM to FM [7, 8, 9, 10]. Photons were also found to destroy the COI state and induce an insulating to metallic transition. The transition is also accompanied by a dramatic change in magnetic property and lattice structure: from COI to ferromagnetic metal (FMM) state [11]. In compounds with a CO state, the lattice is strongly coupled to spin and charge [12]. While charges are ordered, local distortion changes from dynamic Jahn-Teller distortion (JTD) to collective static distortions [12] and the  $\text{MnO}_6$  octahedra buckle up [13].

Under pressure (below  $\sim 2$  GPa), because of the bandwidth  $W$  increase, the CO state can be destroyed and therefore metallic state is induced. Moritomo *et al.* [14] reported that pressure up to 0.8 GPa suppresses CO of the compound  $x = 0.35, 0.4, 0.5$  and  $dT_{co}/dP$  increases with  $x$ . In the  $x = 0.3$  compound, pressure above 0.5 GPa induce a metallic transition which is described as a COI to FMM transition. Magnetic fields were found to be almost equivalent to pressure at least up to 1.5 GPa and can be scaled to pressure.

At present, most of high pressure studies on manganites were carried out in the range below  $\sim 2$  GPa. For studies on metal-insulator transition, in this pressure range, it is found that the FM state and metallic state are coupled, which can be explained qualitatively by double exchange theory [14, 15]. It is generally believed that the application of hydrostatic pressure enhances the hopping integral  $t_0$  leading to a systematic increase of the Curie temperature with pressure. By applying higher pressure, we find that the Curie temperature does not increase monotonically with pressure and does not always couple with the metal insulator transition. In this paper, we report the effects of high pressure (up to  $\sim 6.3$  GPa) on magnetic and electronic properties of a narrow bandwidth manganite,  $\text{Pr}_{0.7}\text{Ca}_{0.3}\text{MnO}_3$ . It was found that in the range of  $\sim 0.8$ -3.5 GPa, pressure induces a metallic state at low temperature and with increasing pressure the transition temperature is increased. The metal-insulator transition (MIT) coincides with the magnetic ordering transition. Above  $\sim 3.5$  GPa,  $T_{MI}$  decreases upon pressure increase. At  $\sim 5$  GPa,  $T_{MI}$  and

magnetic transition temperature start to decouple:  $T_{MI}$  drops much faster than the magnetic transition temperature and finally at  $\sim 6.3$  GPa the sample becomes insulating and the magnetic transition temperature is almost the same as at ambient pressure.

The samples were prepared by solid-state reaction method. Stoichiometric amount of  $\text{Pr}_6\text{O}_{11}$ ,  $\text{MnO}_2$ , and  $\text{CaCO}_3$  were mixed, ground and calcined at  $1100^\circ\text{C}$  for 70 hours; reground and calcined at  $1200^\circ\text{C}$  for 30 hours; the powder was pressed into pellets. The pellets were sintered at  $1350^\circ\text{C}$  for 40 hours and annealed by increasing temperature to  $1350^\circ\text{C}$  and holding it for 10 hours and then slowly cooling to room temperature at the rate of  $1^\circ\text{C}/\text{min}$ . All cycles were performed in air. The X-ray diffraction pattern taken at room temperature shows that the samples are in a single crystallographic phase. The structure was refined to Pbnm symmetry using Rietveld method. The refined lattice parameters are:  $a = 5.4301(1) \text{ \AA}$ ,  $b = 5.4676(1) \text{ \AA}$ ,  $c = 7.6751(1) \text{ \AA}$ . The sample was also characterized by magnetization measurements (FIG. 1). The magnetization as a function of temperature is consistent to that Hwang *et al.* [16] reported. The magnetic moment at 5 K is  $\sim 2.1\mu_B$ , approximate to that reported by Jiráková *et al.* [1]. The details of the high pressure resistivity measurement method were described elsewhere [17].

FIG. 2 gives the temperature dependence of resistivity at different pressures. At ambient pressure, the material is insulating in the whole temperature range. As reported, at a pressure above 0.5 GPa, an insulator to metal transition is induced, which is ascribed to a

COI to FMM transition [14, 16]. With pressure increase, the transition temperature  $T_{MI}$  (defined as the temperature at the resistivity peak) is continuously shifted to higher temperature and resistivity is compressed. In the pressure range 3~4 GPa, this trend saturates. At higher pressure  $T_{MI}$  decreases and the resistivity increases. At ~6.3 GPa, the material becomes insulating in the measured temperature range and the resistivity as a function of temperature almost reproduces the case at ambient pressure. The  $T_{MI}$  vs. pressure is plotted in FIG. 3. The transition temperature of our sample at low pressure is consistent to the result of other authors' polycrystalline samples [16], but is lower than that of single crystals [14] (inset of FIG. 3).

In this doping system, from  $x = 0.1$  to  $0.4$ , the resistivity displays a p-type semiconducting behavior,  $\rho = \rho_0 \exp(E_g / k_B T)$ , with the activation energies ( $E_g$ ) being slightly above 100 meV in the region near room temperature [1]. At ambient pressure, above ~220 K,  $E_g$  is ~125 meV, then increases upon cooling (FIG. 1). Apparently, this  $E_g$  rising corresponds to charge ordering. In the range of 100-130 K,  $E_g$  drops to ~80 meV. According to Jiráček *et al.* [1], the low temperature magnetic state of this compound is composed of ferromagnetic and antiferromagnetic phases, in which the Curie and Néel temperatures are ~115 K and ~130 K, respectively. Hence, by comparing the temperature dependence of resistivity, magnetization and  $E_g$  (FIG. 1), the reduction of  $E_g$  can be correlated with the magnetic transition. Yoshizawa *et al.* [18] reported that with pressure increase up to 2 GPa, the CO and AFM components are gradually reduced and at 2 GPa only FM component presents. Below 0.7 GPa the CO, AFM and FM transitions appear at

different temperature upon cooling. From the  $E_g$  changes and comparison with the magnetization measurement as a function of temperature and Yoshizawa *et al.*'s [18] neutron diffraction result, this  $E_g$  drop can be correlated to the ferromagnetic transition. So we associate the point where  $E_g$  changes fastest with temperature as the ferromagnetic transition temperature  $T_C$ . The transition temperatures extracted at different pressures are plotted in FIG. 3 together with  $T_{MI}$  [the  $T_{MI}$  estimated from ref. 14 (open diamonds) and ref. 16 (solid circles), the  $T_C$  (solid stars) and  $T_N$  (open stars) estimated from the neutron scattering results in ref. 18 are plotted in the inset together with our results for comparison]. It is clearly seen that in the measured pressure range of  $\sim 1.5$ -5 GPa,  $T_C$  and  $T_{MI}$  coincide, indicating that pressure destroys the COI state and induces a FMM state at low temperature. But in the low pressure range and above  $\sim 5$  GPa, the magnetic transition and metal-insulator transition are decoupled and the material becomes insulating at pressures near to ambient pressure and above  $\sim 5$  GPa.

In addition to the magnetic state, the evolution of charge ordering under pressure can also be observed. In the  $E_g$  vs. temperature plots (FIG. 4), rising  $E_g$  corresponds to charge ordering upon cooling disappears gradually with pressure increase and finally the CO state is completely suppressed so that the activation energy does not change with temperature and therefore displays a pure semiconductor behavior above the magnetic transition temperature. Another trend noticeable is the  $E_g$  increasing with pressure above  $\sim 2.8$  GPa in the range near room temperature. In the high pressure range, the activation energy becomes temperature dependent in the paramagnetic phase and decreases upon

cooling. The electron transport cannot be fit to the variable range hopping and polaron hopping models. The origin is not understood.

In the medium pressure range, at the optimum pressure, both the magnetic transition and MIT reach a maximum. This behavior is similar to that observed in the manganites with a larger bandwidth, in which it can be ascribed to the pressure induced Jahn-Teller distortion and Mn-O-Mn bond angle changes according to the double exchange (DE) theory [17, 19, 20].

In the low ( $< \sim 0.8$  GPa) and high ( $> \sim 5$  GPa) pressure range, the material is more insulating and  $T_{MI}$  and  $T_C$  are decoupled. In thin films it was also found that the metal-insulator transition and the magnetic transition decouple [21, 22], in which the decoupling may be ascribed to the strong disorder at  $T_C$  which can be overcome by the magnetization increasing upon cooling so that a metallic state is reached [21]. The  $T_{MI}$  and  $T_C$  decoupling was also reported in the bulk materials  $\text{Pr}_{0.7}\text{Ba}_{0.3}\text{MnO}_3$  [23], in which it is ascribed to the competition between the DE and superexchange (SE) between the Mn-Mn spins. The SE between two neighboring  $\text{Mn}^{3+}$  can either be FM or AFM depending on the Mn-Mn distance [24]. The strength of SE is also a function of the bandwidth  $W$ . At low pressure because of the large lattice distortion,  $W$  is small, SE may dominate and the material displays insulating behavior. With pressure increase, due to the local distortion suppression, DE starts to dominate and hence the insulating state is destroyed, showing

FM metallic state and also  $T_C$  increase with pressure. With pressure increasing, the Mn-Mn distance is monotonically decreased and the local structure distortion of the  $\text{MnO}_6$  octahedra may also changes as in other manganites [17, 19, 20], when it crossovers an optimum value, SE may dominate again. From the resistivity and  $E_g$  vs. temperature plot at  $\sim 6.3$  GPa, the sample seems to be a FM insulator (FMI). The CO phase in the PCMO system is correlated to the lattice distortion, the buckling of the  $\text{MnO}_6$  octahedra [13]. At  $T_{CO}$  a transition from dynamic JTD to collective static distortion takes place [12]. So the CO state disappearance under pressure indicates that the octahedra buckling are compressed and the dynamic distortion dominates at pressure above the optimum pressure.

Mryasov *et al.* [25] indicated that global distortions associated with variations of the apical Mn-O bond length promotes the DE contribution; the bending of the Mn-O bonds in the ab-plane suppresses DE and promotes SE contribution to the interlayer exchange energy.  $\text{La}_{1-x}\text{Sr}_x\text{MnO}_3$  system ( $0.1 \leq x \leq 0.15$ ) also shows a ferromagnetic insulating ground state followed by a canted antiferromagnetic phase at higher temperatures. The ferromagnetic transition is strongly coupled to a structural transition from a Jahn-Teller distorted phase to a pseudocubic orthorhombic phase. Paraskevopoulos *et al.* [26] ascribed it to orbital ordering due to the interplay of superexchange interactions and Jahn-Teller distortions. This AFM-type orbital ordering in the pseudocubic phase can induce an enhancement of the ferromagnetic superexchange interaction, so that magnetic field



can lead to phase transition from FMM phase to FMI phase [27]. So the FMI state above  $\sim 6.3$  GPa could possibly be ascribed to this FM SE interaction enhancement.

In summary, we have measured the electrical resistivity of the small bandwidth manganite  $\text{Pr}_{0.7}\text{Ca}_{0.3}\text{MnO}_3$  as a function of temperature and pressure (ambient to  $\sim 6.5$  GPa). It was found that hydrostatic pressure does not always induce an increase in  $T_C$  and/or  $T_{MI}$  and that the Curie temperature is not always coupled to the metal-insulator transition temperature. In this small bandwidth manganite, pressure induces a metallic state in low temperature region. The metal-insulator transition temperature increases with pressure below  $\sim 3.5$  GPa and decreases above  $\sim 3.5$  GPa and the system becomes a ferromagnetic insulator at higher pressures. In the low ( $< \sim 0.8$  GPa) and high pressure regions ( $> 5$  GPa), the magnetic and electronic transitions are decoupled. In the medium pressure region,  $T_C$  and  $T_{MI}$  coincide and change with pressure as in other manganites with large bandwidth. The pressure effects can be ascribed to the competition between DE and SE interactions and local atomic structure changes with pressure. In addition to magnetic and electronic states, the charge ordering above magnetic transition temperature is found to be suppressed gradually and at high pressure range, an unknown conducting state in paramagnetic is induced. High pressure measurements of the magnetic structure as well as Raman scattering measurements at different temperatures will shed light on the structural origin of these changes in the magnetic structure with pressure. The complex behavior under pressure enables the assessment of the competition between DE and SE (which both depend on bandwidth and atomic structure) without the need for chemical

doping. Hence this system may become a test-bed for studying highly correlated electron systems.

This work is supported by National Science Foundation Grant DMR-0209243.

## CAPTIONS

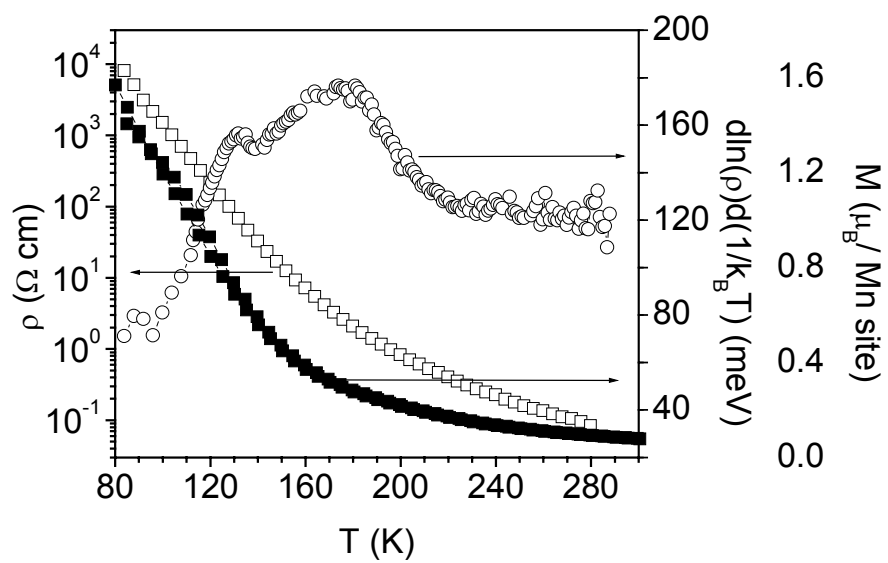
**FIG. 1** Temperature dependence of resistivity, magnetization and activation energy at ambient pressure. Magnetization (solid square) was measured from 4.2 K to 400 (field cooled and zero field cooled) at 10 kOe. The moment at 5 K is  $2.1\mu_B/\text{Mn}$  site. Resistivity is represented by open squares and the open circles represent the activation energy.

**FIG. 2** Temperature dependence of resistivity of  $\text{Pr}_{0.7}\text{Ca}_{0.3}\text{MnO}_3$  at different pressures. The solid and open symbols represent the measurements at pressure below and above the critical pressure respectively.

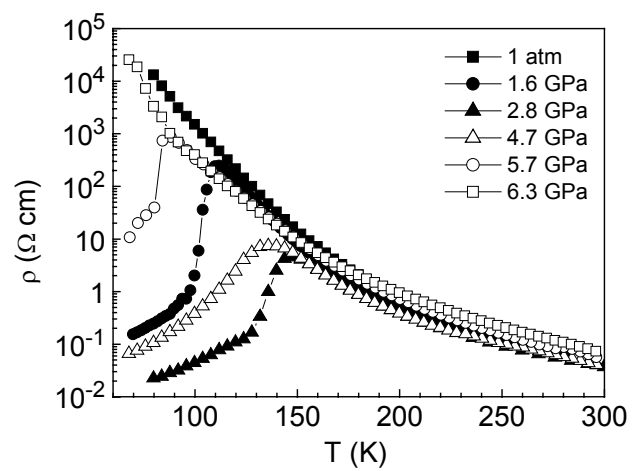
**FIG. 3** Pressure induced transition temperatures. The solid squares represent  $T_{\text{MI}}$ , the solid line is a fit to  $T_{\text{MI}}$  with a third order polynomial for eye-guiding; the open circles represent the  $T_{\text{C}}$  extracted from the activation energy. (In the inset, the results of other authors are displayed for comparison with ours: the solid and open stars are  $T_{\text{C}}$  and  $T_{\text{N}}$  estimated from the neutron scattering result in Ref. 18; The open diamond symbols represent  $T_{\text{MI}}$  estimated from ref. 14, where the sample is single crystal; the solid circles represent  $T_{\text{MI}}$  estimated from ref. 16, where the sample is similar to ours.)

**FIG. 4** Activation energy as a function of temperature at different pressures.  $E_g$  is

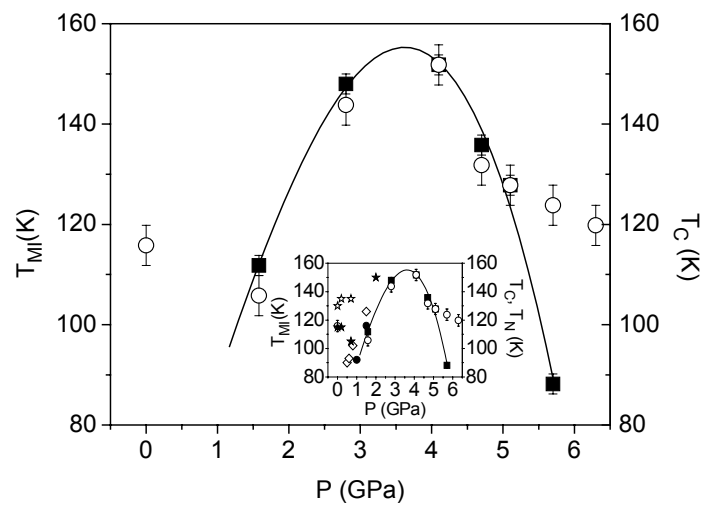
calculated as  $\frac{d \ln(\rho)}{d(k_B T)^{-1}}$  with the resistivity data.



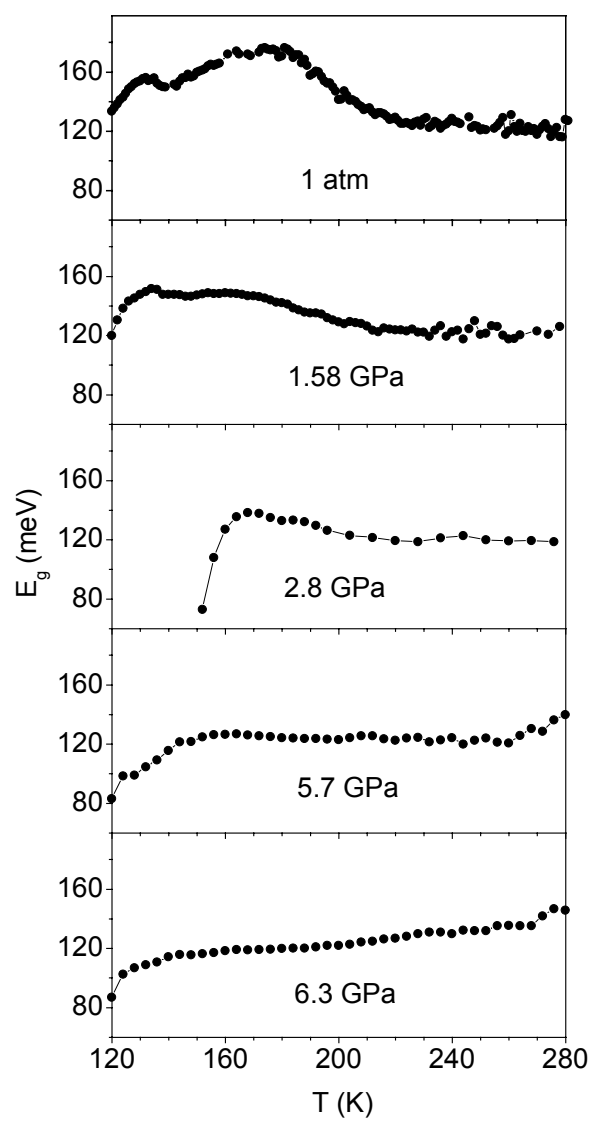
CUI-FIG.1



CUI-FIG.2



CUI-FIG.3



CUI-FIG.4

## REFERENCES

- [1] Z. Jiráček, S. Krupička, Z. Šimša, M. Dlouhá, and S. Vratislav, *J. Magn. and Magn. Mat.* **53**, 153 (1985).
- [2] Y. Tomioka, A. Asamitsu, Y. Moritomo, and Y. Tokura, *J. Phys. Soc. Jpn.* **64**, 3626 (1995).
- [3] A. Asamitsu, Y. Tomioka, H. Kuwahara, and Y. Tokura, *Nature (London)* **388**, 59 (1997).
- [4] V. Kiryukhin, D. Casa, J. P. Hill, B. Keimer, A. Vigliante, Y. Tomioka, and Y. Tokura, *Nature (London)* **386**, 813 (1997).
- [5] D. E. Cox, P. G. Radaelli, M. Marezio, and S-W. Cheong, *Phys. Rev. B* **57**, 3305 (1998).
- [6] K. Miyano, T. Tanaka, Y. Tomioka, and Y. Tokura, *Phys. Rev. Lett.* **78**, 4257 (1997); T. Mori, K. Ogawa, K. Yoshida, K. Miyano, Y. Tomioka, and Y. Tokura, *J. Phys. Soc. Jpn.* **66**, 3570 (1997).
- [7] M. R. Lees, J. Barratt, G. Balakrishnan, D. McK. Paul, and M. Yethiraj, *Phys. Rev. B* **52**, R14303 (1995).
- [8] Y. Tomioka, A. Asamitsu, H. Kuwahara, Y. Moritomo, and Y. Tokura, *Phys. Rev. B* **53**, R1689 (1996).
- [9] M. R. Lees, J. Barratt, G. Balakrishnan, D. McK. Paul, and C. D. Dewhurst, *J. Phys.: Condens. Matter* **8**, 2967 (1996).
- [10] J. Barratt, M. R. Lee, G. Balakrishnan, and D. McK. Paul, *Appl. Phys. Lett.* **68**, 424 (1996).



- [11] V. Kiryukhin, D. Casa, B. Keimer, J. P. Hill, A. Vigliante, Y. Tomioka, and Y. Tokura, *Mat. Res. Soc. Symp. Proc.* **494**, 65 (1998).
- [12] V. Dediu, C. Ferdeghini, F. C. Maticotta, P. Nozar, and G. Ruani, *Phys. Rev. Lett.* **84**, 4489 (2000).
- [13] H. Yoshizawa, H. Kawano, Y. Tomioka, and Y. Tokura, *Phys. Rev. B* **52**, R13145 (1995).
- [14] Y. Moritomo, H. Kuwahara, Y. Tomioka, and Y. Tokura, *Phys. Rev. B* **55**, 7549 (1997).
- [15] J. J. Neumeier, M. F. Hundley, J. D. Thompson, and R. H. Heffner, *Phys. Rev. B* **52**, R7006 (1995).
- [16] H. Y. Hwang, S.-W. Cheong, P. G. Radaelli, M. Marezio, and B. Batlogg, *Phys. Rev. Lett.* **75**, 914 (1995).
- [17] Congwu Cui, Trevor A. Tyson, Zhong Zhong, Jeremy P. Carlo, and Yuhai Qin, *Phys. Rev. B*, in press.
- [18] H. Yoshizawa, R. Kajimoto, H. Kawano, Y. Tomioka, and Y. Tokura, *Phys. Rev. B* **55**, 2729 (1997).
- [19] A. Congeduti, P. Postorino, E. Carmagno, M. Nardone, A. Kumar, and D. D. Sarma, *Phys. Rev. Lett.* **86**, 1251 (2001).
- [20] C. Meneghini, D. Levy, S. Mobilio, M. Ortolani, M. Nuñez-Reguero, Ashwani Kumar, and D. D. Sarma, *Phys. Rev. B* **65**, 012111 (2001).
- [21] J. Aarts, S. Freisem, R. Hendriks, and H. W. Zandbergen, *Appl. Phys. Lett.* **72**, 2975 (1998).

- [22] R. A. Rao, D. Lavric, T. K. Nath, C. B. Eom, L. Wu, and F. Tsui, *J. of Appl. Phys.* **85**, 4794 (1999).
- [23] A. K. Heilman, Y. Y. Xue, B. Lorenz, B. J. Campbell, J. Cmaidalka, R. L. Meng, Y. S. Wang, and C. W. Chu, *Phys. Rev. B* **65**, 214423 (2002).
- [24] J. B. Goodenough, *Phys. Rev.* **100**, 564 (1955).
- [25] O. N. Mryasov, R. F. Sabiryanov, A. J. Freeman, and S. S. Jaswal, *Phys. Rev.* **56**, 7255 (1997).
- [26] M. Paraskevopoulos, F. Mayr, C. Hartinger, A. Pimenov, J. Hemberger, P. Lunkenheimer, A. Loidl, A. A. Mukhin, V. Yu. Ivanov, and A. M. Balbashov, *J. of Magn. and Magn. Mat.* **211**, 118 (2000).
- [27] H. Nojiri, K. Kaneko, M. Motokawa, K. Hirota, Y. Endoh, and K. Takahashi, *Phys. Rev. B* **60**, 4142 (1999).